Using Inverse Electrocardiography to Image Myocardial Infarction

FD Dawoud

Dalhousie University, Halifax, NS, Canada

Abstract

We propose to use methods of inverse electrocardiography (iECG) to compete in the 2007 Computers in Cardiology Challenge, which aims to delineate the location and extent of old myocardial infarct from body-surface potential maps (BSPMs) combined with anatomical imaging information. The provided 120-electrode BSPM data and MRI images were used to calculate epicardial potentials and isochrones of activation. A method was used to define the location and extent of scar tissue based on the morphology of computed epicardial electrograms. Negative Q wave deflection followed by R wave on the left ventricular surface corresponded well with the location of the scar as determined by the gold standard in the two training cases. iECG shows promise as a non-invasive imaging tool to quantitatively characterize location and extent of chronic infarcts.

1. Introduction

Old myocardial infarction (MI) due to a previous episode of ischemia is the most common cause of life-threatening ventricular tachycardia (VT) [1]. Identifying the location of scarred tissue (substrate) is a necessary step to map and terminate the pathway of reentrant activity during the catheter ablation procedure. The aim of the 2007 PhysioNet/Computers in Cardiology Challenge is to establish how well it is possible to characterize the location and extent of moderate to large and relatively compact myocardial infarcts using electrocardiographic evidence supplemented by anatomical imaging information [2]. We propose to use the solution of the inverse problem of electrocardiography in terms of epicardial potentials and isochrones of activation to compete in the Challenge. The non-invasively calculated epicardial potentials and activation sequences have been shown to be in good agreement with normal heart activation during sinus rhythm [3] and to accurately correspond to invasively collected data in torso-tank experiments [4] and during intraoperative mapping [5].

The data provided for the Challenge are body-surface potential maps (BSPMs) collected from four patients (two training cases and two test cases) returning for their one-year follow-up MRI after acute MI as part of the MALT study [6]. Selected MRI sections through the heart were available for all four cases, while gadolinium-enhanced MRI (GE-MRI) images outlining infarction substrate were only provided for the two training cases. Participants of the challenge were asked to estimate the percentage of myocardial mass that is infarcted, the set of myocardial segments containing infarcted tissue according to LV segmentation in [7], and specify the segment containing the center of mass of the infarct scar.

2. Methods

The supplied MRI images (DICOM format) of the four cases were analyzed with Amira 4.1 software (Mercury Computer Systems, Chelmsford, MA) to create customized heart and torso geometries for use in the inverse procedure. Discretized heart surfaces in the four cases consisted of 1000, 700 (Figure 1), 600 and 500 triangular elements, respectively.

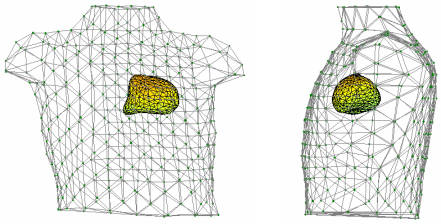

Figure 1. Frontal and left sagittal views of customized torso and epicardial surfaces for case 2. Each surface consists of 700 triangular elements.

Transfer coefficients relating potentials on the epicardium to measured body-surface potentials were calculated with constant interpolating function on triangular elements assuming a homogenous torso. The supplied body-surface ECGs, which were recorded at 120 anatomical locations on the torso according to the standard Dalhousie configuration, were interpolated to the 352 locations corresponding to the standard Dalhousie torso projected on the new customized torso

geometry. The BSPM data contained one averaged PQRST complex sampled at 1000 Hz. The inverse solution was calculated using either Tikhonov 2nd order or 0th order regularization methods and the regularization parameter was obtained according to the *L*-curve method [8]. From the time sequence of calculated epicardial potentials (electrograms), the activation sequences were calculated from the point of electrogram's steepest negative slope. A method was developed to group electrograms based on similar morphology. Electrograms were classified into six categories: QR, qR, Qr, RS, rS and Rs according to the usual nomenclature where Q/q represents early negative deflection, R/r represents positive deflection and S/s represents late negative deflection. Capitalization denotes relative magnitudes of each deflection of the electrogram based on a threshold value chosen to be 0.25. Custom-written MATLAB (Mathworks Inc., Natick, MA) routines were used for all data processing and analysis.

3. Results

Figure 2 shows color-coded distributions of electrogram morphologies for case 2, displayed on the customized heart geometry. The inferior outline of the infarct region as determined from the GE-MRI is shown in gray. Basal parts of the inferior surface of both the RV and LV show QR morphology (blue) while the inferior LV mid-cavity region shows qR morphology (red). It was noticed that infarcted myocardium extents over areas with a major early negative deflection (largely on QR, Qr regions and sometimes on qR). In case 2, a large portion of the infarct occurs on areas showing QR morphology. Presence of QR-type electrograms on basal RV regions could be reflecting infarcted myocardium extending over inferoseptal LV (segments 3 and 9). Figure 3 shows activation times over the epicardial surface. The basal inferior and inferolateral regions show very late activation compared to surrounding tissue, suggesting the presence of infarction.

Figure 4 shows distribution of the electrograms morphology for case 1, where the infarct was located primarily in the septum (segments 1, 2, 3, 8, 9, 13, 14 and 15). A region of QR pattern is seen overlaying the anterior interventricular groove, extending slightly laterally towards the LV and RV. On the inferior surface, a reciprocal morphology of RS deflection (green) overlays the groove. Electrogram morphologies on the LV appear to have inverted mirror images on the RV, i.e. qR (red) on LV reflects as rS (light blue) on RV, Rs (black) on LV reflects as Qr (yellow) on RV. Figure 5 shows activation times for case 1 where crowding of isochronal lines can be seen on the antero-superior groove as well as on the inferoseptal regions of the epicardial surface extending from base to apex, which can be explained by the presence of septal infarct.

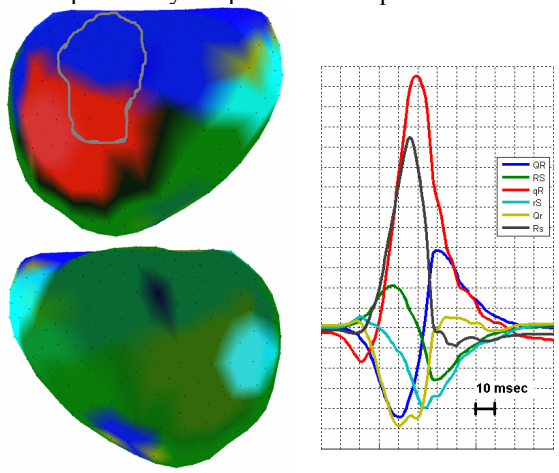

Figure 2. Inferior (top left) and anterior (bottom left) views of case 2 epicardial surface color-coded according to average electrogram types (right). Inferior portion of infarct obtained from GE-MRI is outlined in gray.

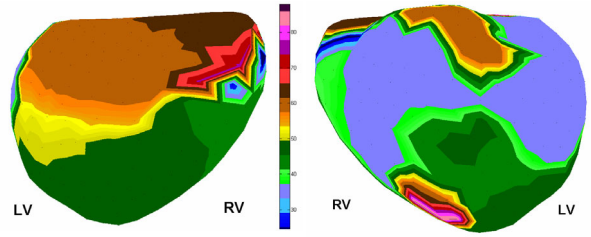

Figure 3. Isochrones of activation on the antero-superior (right) and inferior (left) epicardial surface in reference to QRS onset for case 2. A region of late activation occurs on basal inferior/inferolateral LV, which corresponds to known location of infarction.

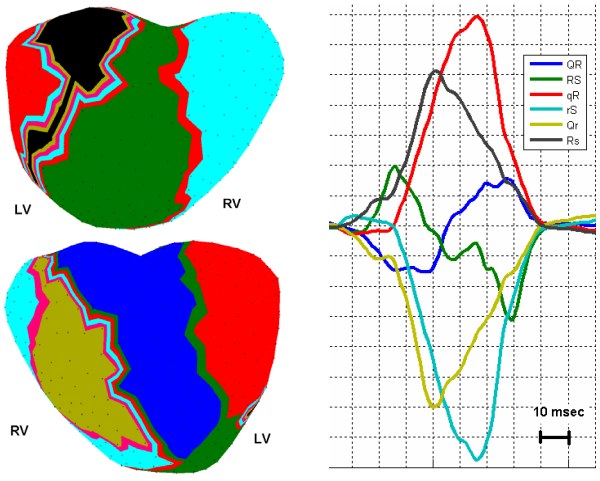

Figure 4. Case 1 electrogram morphology results. Format is the same as in Fig 2.

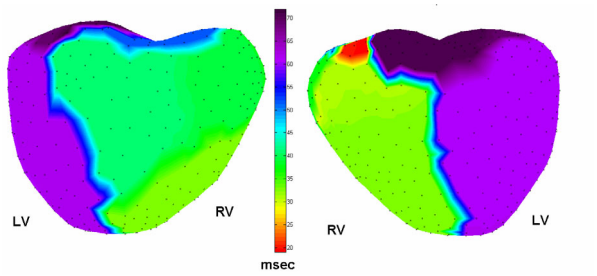

Figure 5. Isochrones of activation for case 1 showing slowed conduction depicted as crowding of isochrones over the anterior interventricular groove (right) and very close to inferior groove (left).

Based on results obtained from the training cases 1 and 2, criteria for determining the location and centroid of the underlying infarction was based on the presence of major Q wave morphology of electrograms combined with the presence of regions of condensed isochrones or very late activation times. Extent of the infarction was qualitatively estimated using weights assigned to segments based on the spread of estimated infarct in the segment and relative size of the segment.

Figures 5 and 6 show results obtained using the morphology classification method and the activation time map. Region of QR morphology overlays basal as well as mid-cavity inferior/inferolateral parts of the LV. Late activation times appear at a similar location. Extension of QR-type electrograms over the inferior RV base suggests (as seen in case 2 results) basal inferoseptal spread of the infarct. Segments estimated to contain infarct were 3, 4, 5, 10 and 11 (scored 0.556 out of 1) with centroid located in segment 4 (1 segment away) extending over 35% of LV mass (departing 17% from gold standard reference).

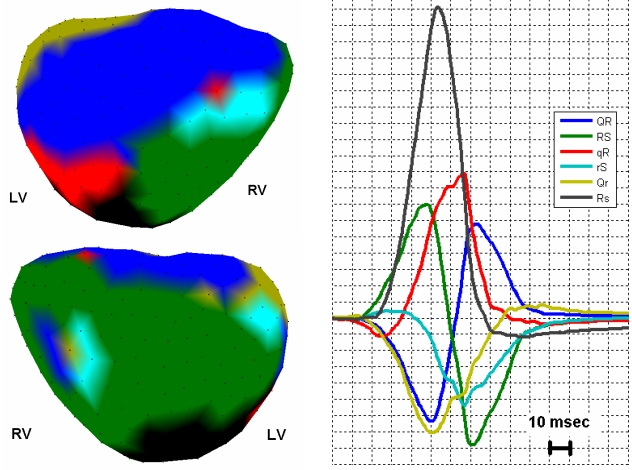

Figure 6. Case 3 electrogram morphologies. Format is the same as in Fig. 2

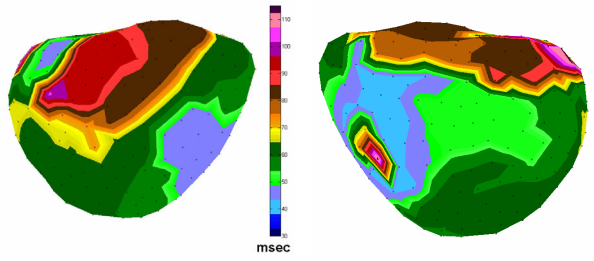

Figure 7. Case 3 activation times map on the inferior (left) and antero-superior (right) surfaces of the heart showing late activation times and condensed isochrones on the basal inferior LV extending to mid-cavity inferolateral region.

Results for case 4 are shown in Figures 8 and 9. Region of QR morphology appears on basal RV and LV extending towards antero-lateral LV. qR morphology is seen on the remainder of the inferior surface, similar to case 2. Late activation occurs in regions with QR morphology. Estimated infarcted segments were 3, 4, 5, 6, 9, 10, 11 (scored 0.333 out of 1), with centroid located in segment 4 (2 segment away) extending over 40% of LV mass (departing 26% from gold standard reference).

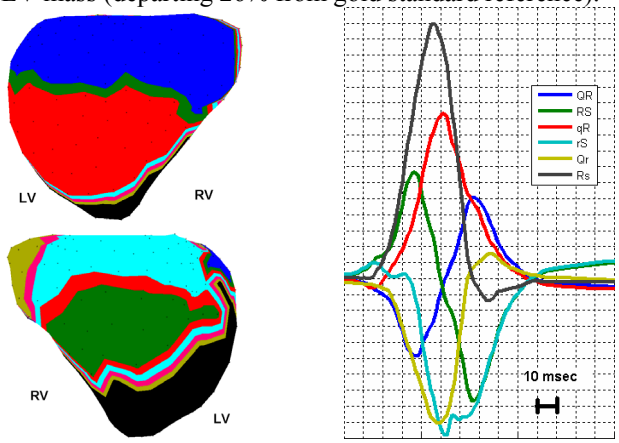

Figure 8. Case 4 electrogram morphologies. Format is the same as in Fig. 2

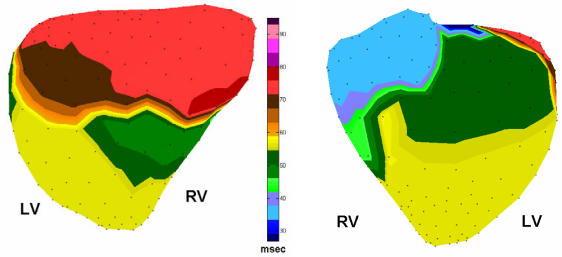

Figure 9. Case 4 inferior (left) and antero-superior (right) activation time map.

4. Discussion and Conclusions

The inversely calculated epicardial potentials using body-surface potential mapping data and a transfer matrix constructed from customized torso and heart geometries provide a rationale way to image local epicardial activity based on a physiological approach. The two methods that were used to localize old myocardial infarct show agreement and consistency in the two training cases. Displaying regions of similar electrogram morphology would appear to be a useful way to summarize progression of electrical activation in one map. The appearance of Q wave-type electrograms (Qr, QR and qR) on the LV was observed to correspond to infarcted areas. This result is consistent with clinical presentation of abnormal deep and wide Q waves in certain 12-lead ECG leads in cases of old MI. It is interesting to note that in case 4, which did not present any abnormal Q waves in 12-ECG leads, the inversely calculated heart electrograms still indicated areas with QR morphology over LV inferobasal regions.

Calculated isochronal maps showed areas of late activation or crowding of isochrones close to the infarct region. The extent of the infarct as estimated by the isochrone maps tended to be more localized, while the electrogram-morphology method tended to overestimate the infarcted region. This can be overcome by adding additional amplitude, slope, integration or duration constraints to the currently simple criterion of relative peak amplitude of 0.25 used to classify electrograms. Other methods were attempted (results not shown) to infer location of infarct with different degrees of success. These include QRS integral, peak positive depolarization amplitude, steepest negative slope value during depolarization and J-point elevation. These criteria would need to be tested more systematically on a large number of cases to evaluate their effectiveness and determine appropriate threshold values for infarcted tissue.

There are some limitations for applying the inverse solution method, particularly on a large scale. Most important is the sensitivity of the inversion procedure to geometrical errors introduced by inaccurate orientation of the heart surface and uncertainty about body-surface lead locations. Constructing accurate geometries is time-consuming and entails additional cost of using scans from a non-invasive imaging modality. Another limitation relates to tendency of the inverse procedure to preserve electrogram amplitudes less accurately than morphology, which prompted our approach to use a pattern-oriented algorithm to classify electrograms.

In conclusion, our method of approximating infarct location and extent using an inverse procedure with customized torso and heart geometries shows promise and warrants further validation on control cases (free from MI) to establish normal electrogram patterns and distribution as well as on MI cases to investigate variability, evaluate accuracy and improve detection algorithms.

Acknowledgements

The author would like to thank Drs. Milan Horacek and John Sapp for their supervision and acknowledges the financial support from the Nova Scotia Heart and Stroke Foundation and the Canadian Institute of Health Research.

References

[1] Stevenson WG. Ventricular tachycardia after myocardial infarction: from arrhythmia surgery to catheter ablation.. J Cardiovasc Electrophysiol (1995) **6**: pp. 942-950.

[2] PhysioNet. PhysioNet/Computers in Cardiology Challenge 2007: Electrocardiographic Imaging of Myocardial Infarction. [homepage on the internet]. Cambridge, MA: PhysioNet; [updated 2007 September 21; cited 2007 September 23]. Available from: http://physionet.org/challenge/2007/

[3] Ramanathan C, Jia P, Ghanem R, Ryu K & Rudy Y. Activation and repolarization of the normal human heart under complete physiological conditions.. Proc Natl Acad Sci U S A (2006) **103**: pp. 6309-6314.

[4] Oster HS, Taccardi B, Lux RL, Ershler PR & Rudy Y. Noninvasive electrocardiographic imaging: reconstruction of epicardial potentials, electrograms, and isochrones and localization of single and multiple electrocardiac events.. Circulation (1997) **96**: pp. 1012-1024.

[5] Ghanem RN, Jia P, Ramanathan C, Ryu K, Markowitz A & Rudy Y. Noninvasive electrocardiographic imaging (ecgi): comparison to intraoperative mapping in patients.. Heart Rhythm (2005) **2**: pp. 339-354.

[6] Engblom H, Foster JE, Martin TN, Groenning B, Pahlm O, Dargie HJ, Wagner GS & Arheden H. The relationship between electrical axis by 12-lead electrocardiogram and anatomical axis of the heart by cardiac magnetic resonance in healthy subjects.. Am Heart J (2005) **150**: pp. 507-512.

[7] M.D. Cerqueira, N.J. Weissman, V. Dilsizian, A.K. Jacobs, S. Kaul, et al. Standardized myocardial segmentation and nomenclature for tomographic imaging of the heart. Circulation, 105:539-542, 2002.

[8] Per Christian Hansen. Analysis of discrete ill-posed problems by means of the l-curve. SIAM Review (1992) **34**: pp. 561-580.

Address for correspondence:

Fady Dawoud
4P-1 5859 University Avenue
Halifax, NS, B3H4H7
fdawoud@dal.ca